Supplemental material

NMR reveals the intrinsically disordered domain 2 of NS5A protein as an allosteric regulator of the hepatitis C virus RNA polymerase NS5B

Luiza M. Bessa, Hélène Launay, Marie Dujardin, François-Xavier Cantrelle, Guy Lippens, Isabelle Landrieu, Robert Schneider and Xavier Hanoulle

From the University of Lille, CNRS, UMR 8576, UGSF, Unité de Glycobiologie Structurale et Fonctionnelle, F 59000 Lille, France

Contents:

Figure S1: $^{1}H,^{13}C$ methyl-TROSY spectra of Ile-to-Val mutants of $NS5B_{\Delta 21}$ used for assignment of Ile δ1 methyl resonances.

Figure S2: Examples of inter-methyl NOEs used in the assignment of $NS5B_{\Delta 21}$ Ile δ1 methyl resonances.

Figure S3: NMR chemical shift predictions from NS5B X-ray structures.

Figure S4: Isoleucine side chain $\chi 2$ dihedral angles extracted from NS5B crystallographic structures.

Figure S5: Comparison of experimental $NS5B_{\Delta 21}$ Ile methyl-δ1 chemical shifts with predicted values.

Figure S6: Effect of static B_0 magnetic field on the NS5B spectrum.

Figure S7: Methyl-TROSY MQ CPMG relaxation dispersion data for $NS5B_{\Delta 21}$ Ile δ1 methyl resonances.

Figure S8: Thermal shift analysis of NS5B.

Figure S9: Control experiments for a potential interaction between NS5A-D2 and RNA16.

Figure S10: NMR analysis of the $NS5B_{\Delta 21}$ L30S mutant.

Figure S11: NMR analysis of $NS5B_{\Delta 60}$.

Figure S12: NMR analysis of the $NS5B_{\Delta 21}$ 5mut mutant.

Table S1: NOEs between Ile δ1-methyl groups in $NS5B_{\Delta 21}$.

Table S2. ^{1}H and ^{13}C chemical shifts for isoleucine δ1-methyl groups in $NS5B_{\Delta 21}$.

Table S3. NS5B residues whose NMR resonances are affected by Ile-to-Val point substitution.

Table S4. NS5B crystallographic structures used to extract dihedral angles and to predict NMR chemical shifts.

Table S5: Parameters resulting from fits of models of two-state exchange to methyl-TROSY MQ CPMG relaxation dispersion data.

Figure S1

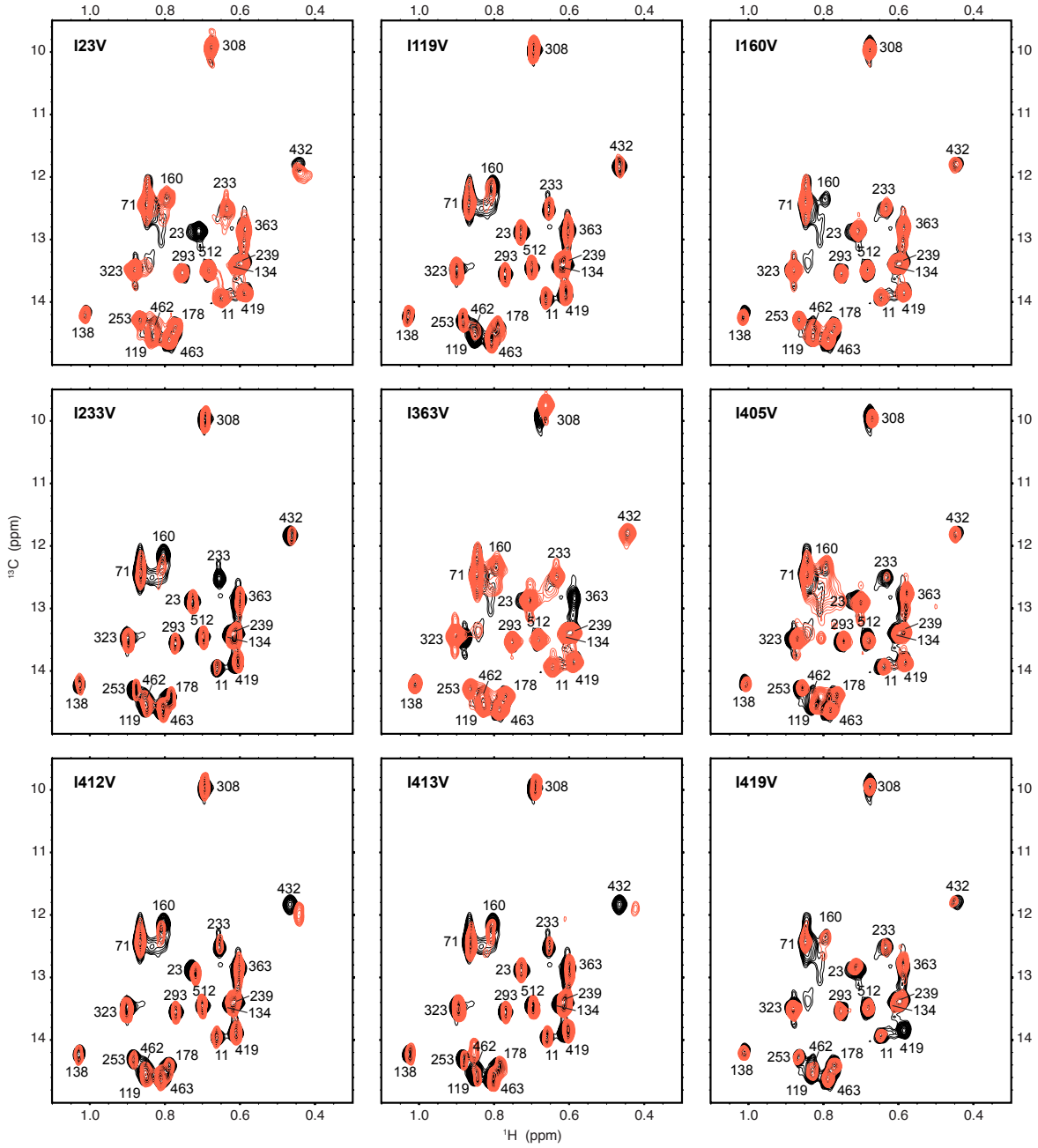
I23V
I119V
I160V
I233V
I363V
I405V
I412V
I413V
I419V
308
432
160
233
71
23
363
293
512
239
134
323
462
178
11
419
253
138
119
463
^{13}C (ppm)
^{1}H (ppm)

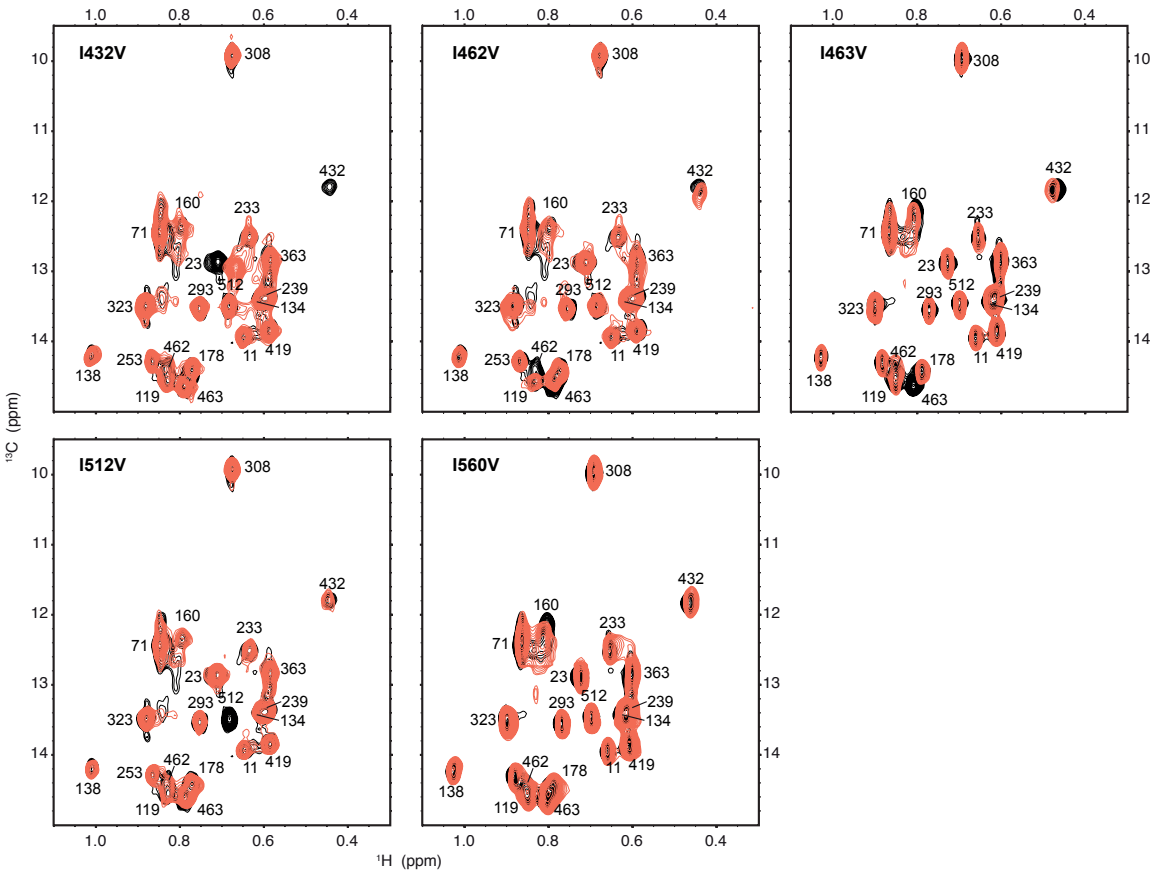

Figure S1. Assignment of the ^{1}H,^{13}C 2D methyl TROSY spectrum of [$^{13}C_{\delta1}{}^{1}H_3$]-Ile, U-^{2}H labelled NS5B$_{\Delta21}$ from the HCV JFH1 strain. Each panel corresponds to the superposition of the spectrum of NS5B$_{\Delta21}$ (in black) and the spectrum of an Ile-to-Val NS5B$_{\Delta21}$ mutant (in red). Spectra were acquired at 900 MHz ^{1}H Larmor frequency in either phosphate buffer (WT, I23V, I405V, I419V, I432V, I462V, I512V) or in R/E buffer (WT, I119V, I233V, I412V, I413V, I463V, I560V).

Figure S2

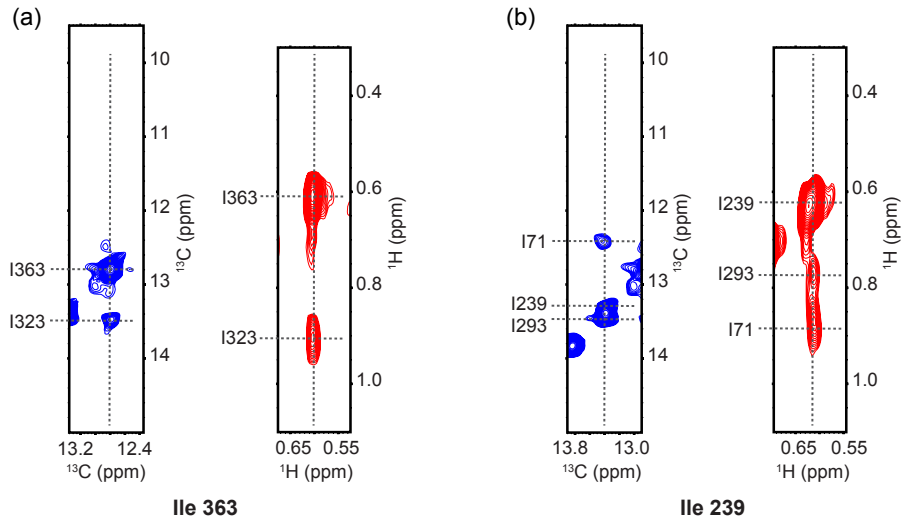

Figure S2. Intramolecular NOEs between Ile δ1-methyl groups in NS5B$_{\Delta 21}$. (a) Strips of Ile 363 CH_3-δ1 extracted at 0.605 ppm from the ^{13}C-edited 3D HMQC-NOESY-HMQC spectrum (left) and at 12.809 ppm from the ^{13}C-edited 3D NOESY-HMQC spectrum (right). (b) Strips of Ile 239 CH_3-δ1 extracted at 0.609 ppm from the ^{13}C-edited 3D HMQC-NOESY-HMQC spectrum (left) and at 13.385 ppm from the ^{13}C-edited 3D NOESY-HMQC spectrum (right). Spectra were acquired with a 900 MHz spectrometer.

Figure S3

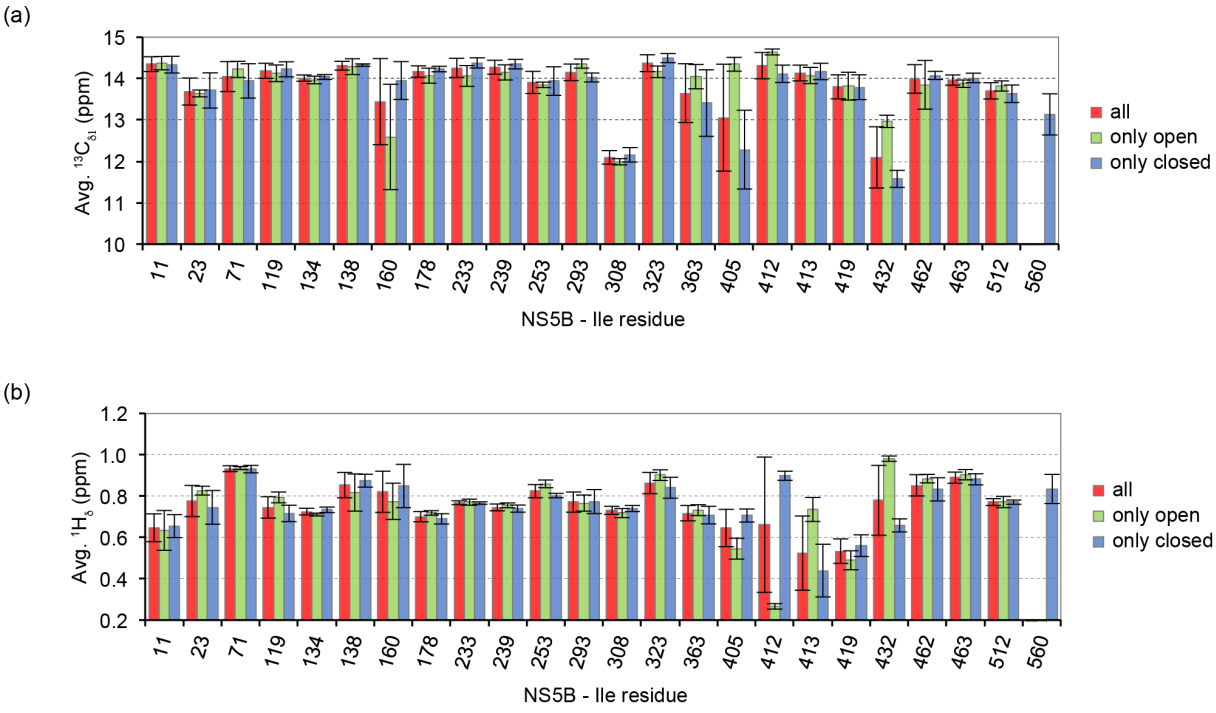

Figure S3. NMR chemical shift predictions from NS5B X-ray structures. ^{13}C (a) and ^{1}H (b) chemical shift predictions for Ile δ1-methyl groups in $NS5B_{\Delta 21}$ were performed on the NS5B crystallographic structures listed in **Table S4**, using the software SHIFTX2 (1). Predictions are presented as average values (ppm ± SD) from all (in red), only open (in green) and only closed (in blue) NS5B conformations.

Figure S4

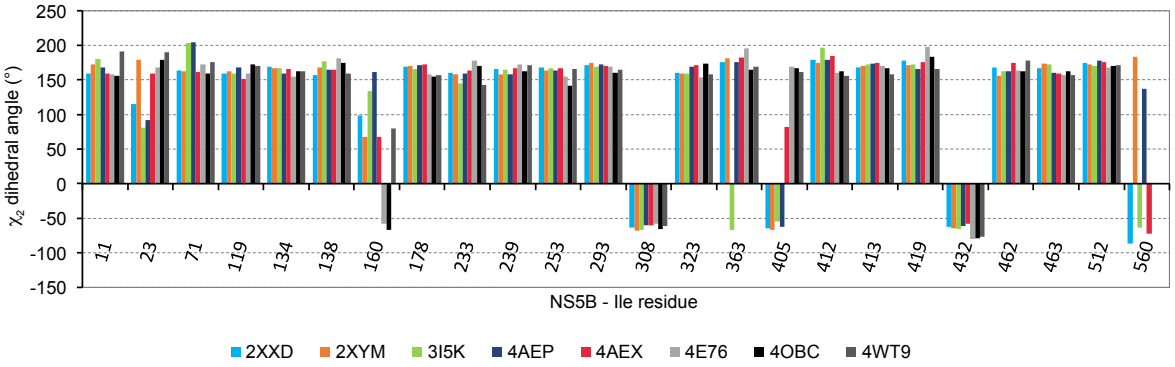

Figure S4. Isoleucine side chain $\chi 2$ dihedral angles (° deg.) extracted from the NS5B crystallographic structures listed in **Table S4**.

Figure S5

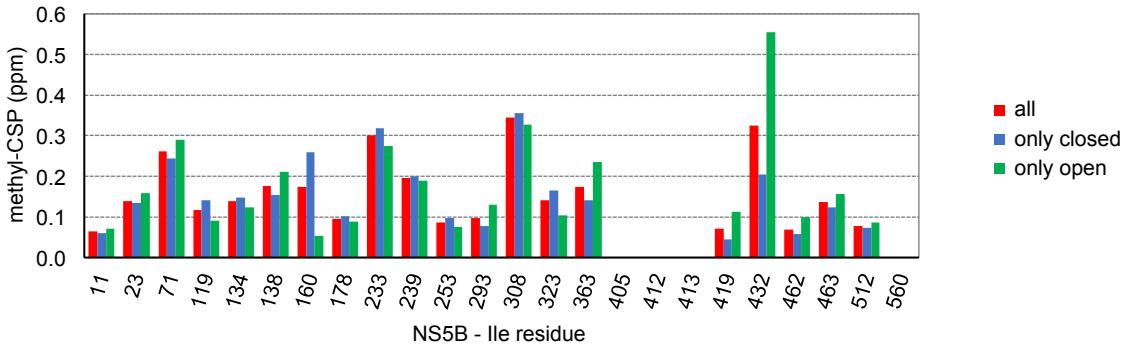

Figure S5. Comparison of experimental NS5B$_{\Delta 21}$ Ile methyl-δ1 chemical shifts with predicted values. Deviations (ppm) between experimental and predicted values were calculated as $^{1}H,^{13}C$ combined chemical shift perturbations (CSP, in ppm; see Equation 1 in the main text) between experimental and average SHIFTX2-predicted values for all (red), only open (green), and only closed (blue) NS5B crystallographic structures, as listed in **Table S4**.

Figure S6

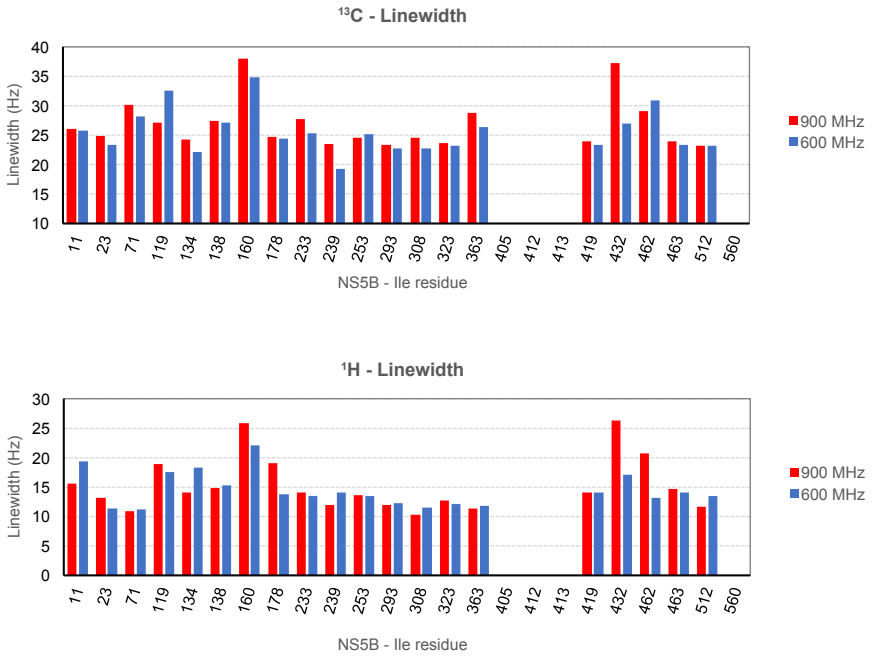

Figure S6. Effect of static B_0 magnetic field on the NS5B spectrum. Linewidths at half-height in the ^{13}C dimension (top) and in the ^{1}H dimension (bottom) of Ile methyl (δ1) groups in $^{1}H,^{13}C$ TROSY spectra of $NS5B_{\Delta 21}$ acquired either at 600 (in blue) or at 900 MHz (in red) are shown. Spectra were processed without apodization.

Figure S7

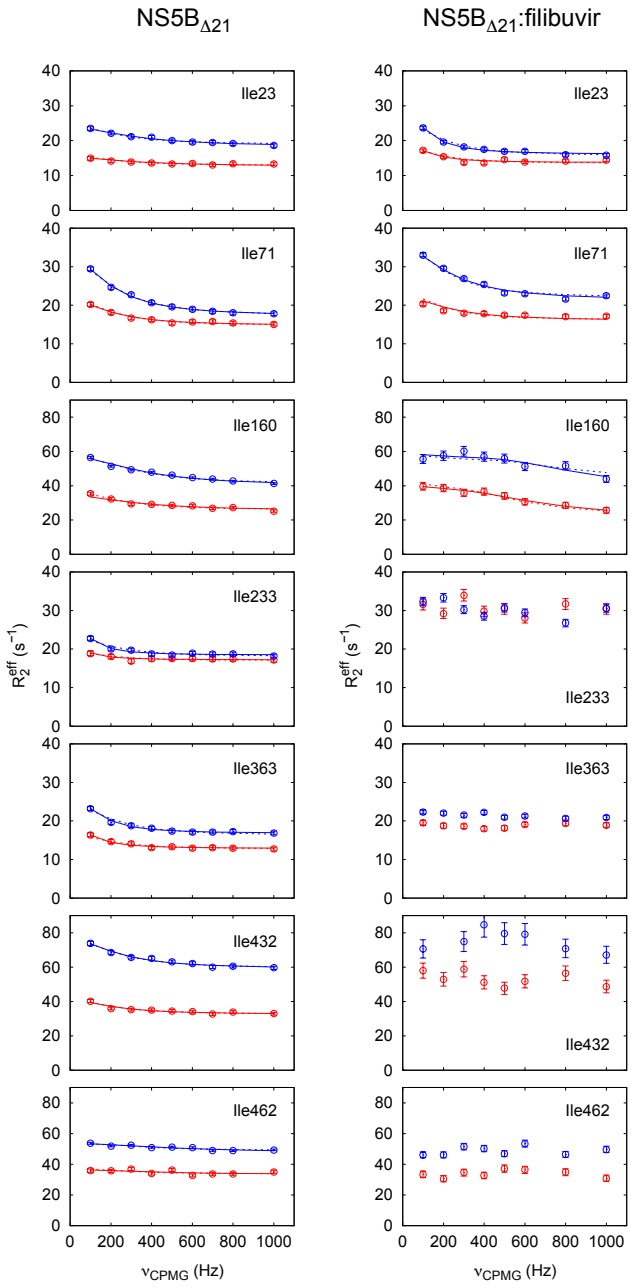

Figure S7. Methyl-TROSY MQ CPMG relaxation dispersion data for all NS5B$_{\Delta21}$ Ile residues that, in apo NS5B$_{\Delta21}$, exhibit significant exchange contributions to their transverse relaxation rate $R_{2,eff}$ (i.e. non-flat dispersion curves) according to F test statistics. Red, 600 MHz; blue, 900 MHz; left column, apo NS5B$_{\Delta21}$; right column, NS5B$_{\Delta21}$ in the presence of filibuvir. Solid lines represent best fits to individual residue data where significant dispersion is present; dashed lines represent grouped fits to all residues exhibiting dispersion of each state (apo and with filibuvir, respectively) together. Individual-residue fits allowed ^{1}H and ^{13}C $\Delta\omega$ to vary for residues 23, 71, 233, and 432 in apo NS5B$_{\Delta21}$ and for residue 71 in NS5B$_{\Delta21}$ with filibuvir; for the other residues, ^{1}H $\Delta\omega$ was fixed to zero. Grouped fits always allowed both ^{1}H and ^{13}C to vary. For resultant fit parameters, see Table S5.

Figure S8

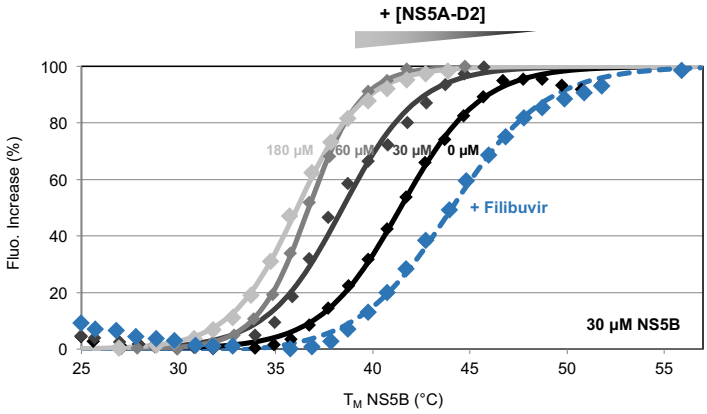

Figure S8. Thermal shift analysis of NS5B. SYPRO Orange fluorescence increase as function of temperature for $NS5B_{\Delta 21}$ (30µM) mixed with increasing concentrations of NS5A-D2 (0, 30, 60 and 180µM, grey to black curves) and for the $NS5B_{\Delta 21}$:filibuvir complex (blue curve).

Figure S9

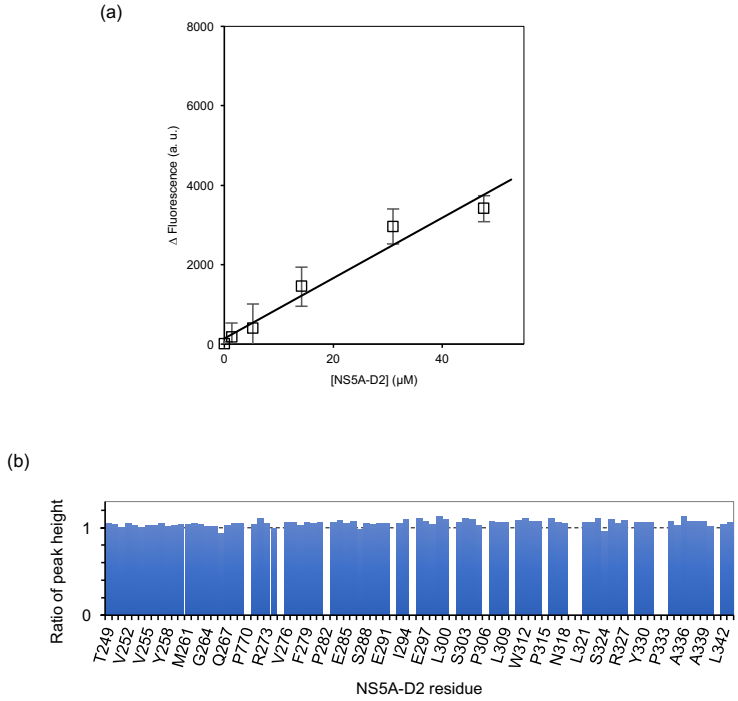

Figure S9. Control experiments for a potential interaction between NS5A-D2 and RNA16. (Top) Fluorescence spectroscopy. Titration of a fluorescent RNA oligonucleotide (6FAM-RNA16, 50 nM) with increasing concentrations of NS5A-D2 (from 1.3 to 47 μM). The increase in fluorescence intensity (515 – 525 nm) of 6FAM-RNA16 is plotted as a function of NS5A-D2 concentration. Error bars represent one standard deviation of three replicates. (Bottom) NMR spectroscopy. A $^{1}H,^{15}N$-HSQC NMR spectrum of ^{15}N-NS5A-D2 (50 μM) in the presence of RNA16 (1:1 ratio) was acquired. For each NS5A-D2 residue, the intensity (peak height) of its NMR resonance is shown as a blue bar, normalized by the intensity observed in a spectrum recorded in the absence of RNA16.

Figure S10

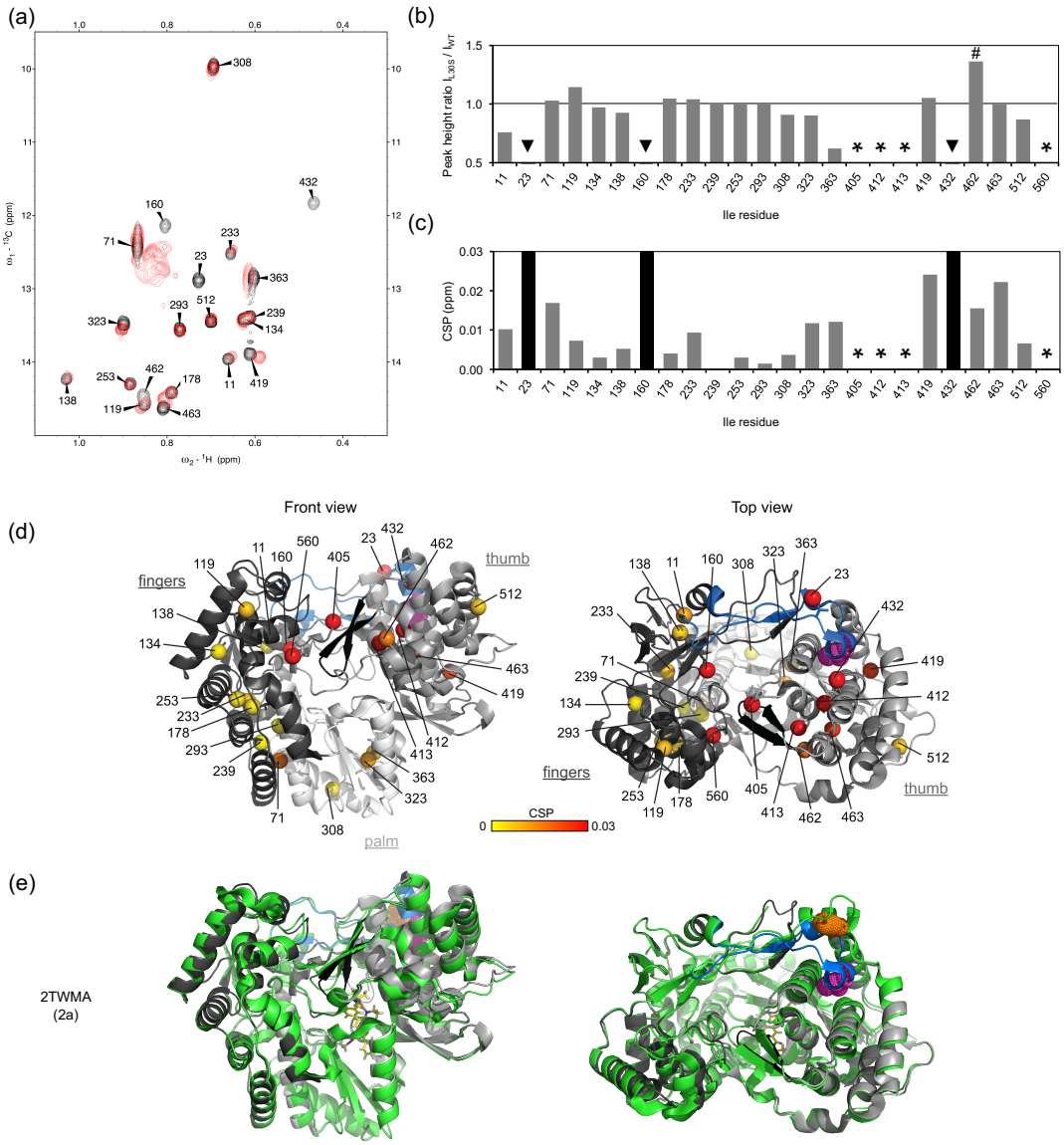

Figure S10. NMR analysis of the NS5B$_{\Delta 21}$ L30S mutant. (a) Superposition of methyl-TROSY spectra of NS5B$_{\Delta 21}$ (in black) and the NS5B$_{\Delta 21}$ L30S mutant (in red). (b) Peak intensity ratios (I_{L30S}/I_{WT}) of Ile methyl (δ1) groups of NS5B measured both for NS5B$_{\Delta 21}$ and for the NS5B$_{\Delta 21}$ L30S mutant. For each spectrum, relative peak intensities are normalized to the Ile 293 signal. Residues whose resonances were not observed in any spectra are highlighted by a black asterisk (∗). Residues that were only observed in the NS5B$_{\Delta 21}$ WT spectrum are indicated by a black triangle (▼). The Ile462 resonance in the NS5B$_{\Delta 21}$ L30S mutant spectrum is mainly overlapped with that of Ile 119 and is indicated with a # symbol. (c) ^{1}H,^{13}C combined chemical shift perturbations (CSP) triggered by the L30S mutation for Ile methyl (δ1) groups of NS5B. Residues whose resonances were not observed in any spectra are highlighted by a black asterisk (∗). Residues only observed in the NS5B$_{\Delta 21}$ WT spectrum are indicated by a black bar. (d) ^{1}H,^{13}C combined chemical shift perturbations (CSP) triggered by the L30S mutation are mapped, from yellow (0 ppm) to red (0.03 ppm), onto the Ile methyl groups of the NS5B structure (PDB ID: 2XXD). Methyl groups that were not observed are depicted in red. (e) Superposition of the crystallographic structures of NS5B (JFH1) (PDB ID:

2XXD) (in grey) and of the NS5B L30S mutant (PDB ID: 2WTM) (in green) in the presence of a palm inhibitor (shown as yellow sticks). Residue L30 in the NS5B structure is shown in pink and is localized at the apex of the fingertips loop Λ1 shown in blue. The L30S mutation is shown in orange on the structure of the NS5B L30S mutant. The fingertips loop Λ1 is displaced from the thumb subdomain in the L30S mutant.

Figure S11

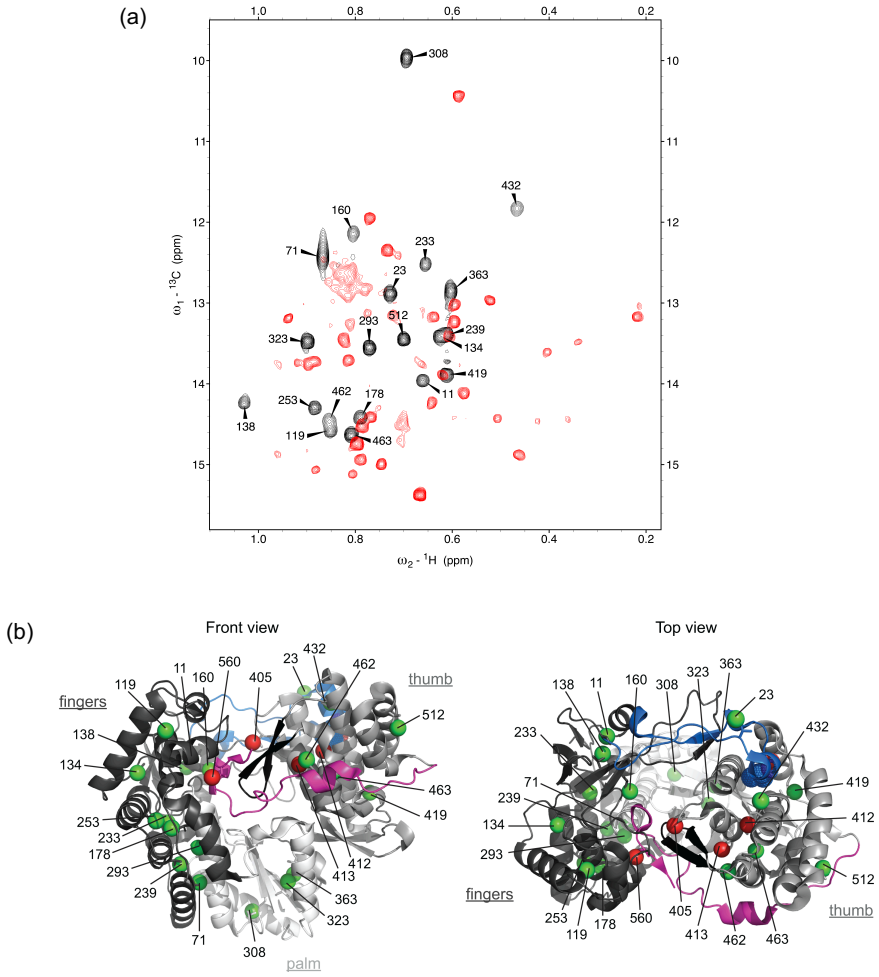

Figure S11. NMR analysis of NS5B$_{\Delta 60}$. (a) Superposition of methyl-TROSY spectra of NS5B$_{\Delta 21}$ (in black) and NS5B$_{\Delta 60}$ (in red). (b) The C-terminal deletion in the Δ60 mutant is highlighted in pink on the crystallographic structure of NS5B (JFH1) (PDB ID: 2XX). The fingertip Λ1 is shown in blue. Methyl (δ1) groups of Ile residues are shown as spheres and are coloured in green if the corresponding resonances were observed in the NMR spectrum of NS5B$_{\Delta 21}$ and in red otherwise.

Figure S12

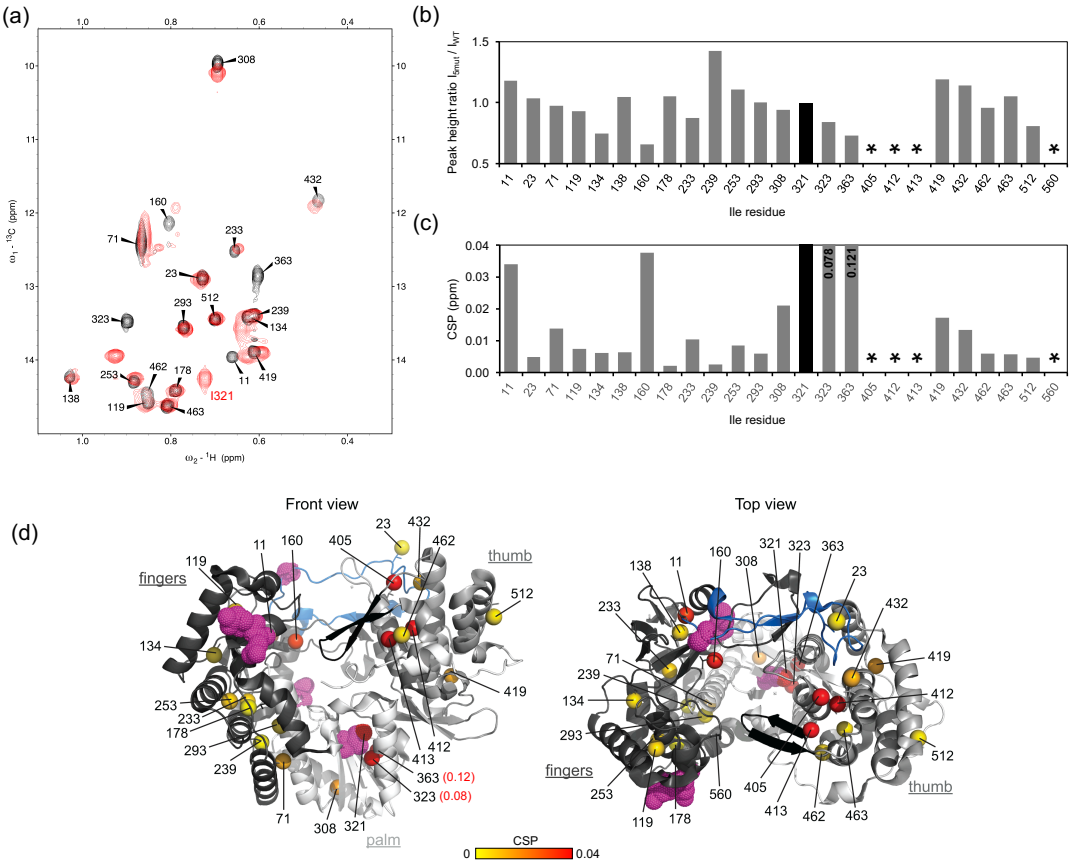

Figure S12. NMR analysis of the NS5B$_{\Delta21}$ 5mut mutant. (a) Superposition of methyl-TROSY spectra of NS5B$_{\Delta21}$ (in black) and of the NS5B$_{\Delta21}$ 5mut mutant (in red), which contains S15G, E86Q, E87Q, C223H and V321I mutations. The supplemental Ile methyl resonance corresponding to Ile 321 in the NS5B$_{\Delta21}$ 5mut spectrum is labelled in red. (b) Peak intensity ratios (I_{5mut}/I_{WT}) of Ile methyl (δ1) groups of NS5B measured both for NS5B$_{\Delta21}$ and for the NS5B$_{\Delta21}$ 5mut mutant. For each spectrum, relative peak intensities are normalized to the Ile293 signal. Residues whose resonance was not observed in any spectrum are highlighted by a black asterisk (∗). The intensity ratio for the additional I321 residue (only present in the NS5B$_{\Delta21}$ 5mut mutant) was arbitrarily set to 1 and is shown as a black bar. (c) ^{1}H,^{13}C combined chemical shift perturbations (CSP) triggered by the 5 mutations for Ile methyl (δ1) groups of NS5B. The value for the additional Ile 321 residue (only present in the NS5B$_{\Delta21}$ 5mut mutant) was arbitrarily set to 1 and is shown as a black bar. CSPs for Ile 323 and Ile 363 are 0.078 ppm and 0.0121 ppm, respectively, values which are above the defined upper limit and thus are reported in the figure. (d) ^{1}H,^{13}C combined chemical shift perturbations (CSP) triggered by the 5 mutations (5mut) are mapped, from yellow (0 ppm) to red (0.04 ppm), onto the Ile methyl groups of the NS5B structure (PDB ID: 2XXD). Methyl groups that were not observed are depicted in red. Residues S15, E86, E87, C223, and V321 which are mutated in the 5mut mutant are shown in pink.

Table S1

Residue	NOE with residue(s)	Distance (Å) in X-ray structure
Ile 11	Ile 138	4.15
Ile 71	Ile 239	5.42
Ile 138	Ile 11	4.15
Ile 178	Ile 253	3.58
Ile 239	Ile 71, Ile 293	5.42, 5.52
Ile 253	Ile 278	3.58
Ile 293	Ile 239	5.52
Ile 323	Ile 363	4.52
Ile 363	Ile 323	4.52
Ile 462	Ile 463	7.49
Ile 463	Ile 462	7.49

Table S1. NOEs between Ile δ1-methyl groups in [$^{13}C_{\delta1}{}^{1}H_3$]-Ile, U-$^{2}H$ labelled $NS5B_{\Delta21}$ from the JFH1 HCV strain and their corresponding distances (Å) in the crystallographic structure of NS5B (PDB ID: 2XXD).

Table S2

Residue	^{1}H (δ1) (ppm)	^{13}C (δ1) (ppm)
Ile 11	0.66	13.97
Ile 23	0.72	12.88
Ile 71	0.86	12.46
Ile 119	0.84	14.59
Ile 134	0.62	13.42
Ile 138	1.03	14.24
Ile 160	0.81	12.34
Ile 178	0.79	14.44
Ile 233	0.65	12.52
Ile 239	0.61	13.41
Ile 253	0.88	14.31
Ile 293	0.77	13.55
Ile 308	0.69	9.91
Ile 323	0.89	13.51
Ile 363	0.60	12.82
Ile 405	*n.d.*	*n.d.*
Ile 412	*n.d.*	*n.d.*
Ile 413	*n.d.*	*n.d.*
Ile 419	0.60	13.86
Ile 432	0.46	11.79
Ile 462	0.84	14.45
Ile 463	0.80	14.64
Ile 512	0.70	13.52
Ile 560	*n.d.*	*n.d.*

n.d.: not determined, the resonance was not observed in spectra

Table S2. ^{1}H and ^{13}C chemical shifts for isoleucine δ1-methyl groups in NS5B$_{\Delta 21}$ from the JFH-1 HCV strain (genotype 2a).

Table S3

Mutation	CSP	Height increase	Height decrease
I23V	432	160	
I119V	419	138	
I160V	138, 462		
I233V	160	119, 512	
I363V	308, 323		462
I405V	462, 363		134, 178, 233, 253, 308, 512
I412V	432, 23, 160	432	
I413V	160, 432, 462, 419	462	
I419V	363		119
I432V	23		
I462V	432, 463		119
I463V	160, 462, 432		
I512V			
I560V	160, 419		

Table S3. NS5B residues whose NMR resonances are affected by Ile-to-Val point substitution. Several parameters were observed: ^{1}H and ^{13}C combined chemical shift perturbation (CSP) and changes in normalized data height. Values in the table correspond to residue numbers. Residues with CSPs above 0.015 ppm are indicated in black and those with 0.010 < CSP < 0.015 ppm in grey. Height increase, data height > 150% of wild-type $NS5B_{\Delta 21}$; height decrease, data height < 75% of wild-type $NS5B_{\Delta 21}$.

Table S4

PDB structure ID	Inter-subdomain angle (°)	Template channel width (Å)	NS5B conformation
2XXD	68.80	16.59	closed
2XYM	66.84	16.15	closed
3I5K	68.82	15.87	closed
4AEP	68.29	16.56	closed
4AEX	69.19	16.07	closed
4E76	75.91	26.02	open
4OBC	74.31	25.94	open
4WT9	75.44	26.15	open

Table S4. NS5B crystallographic structures used to extract dihedral angles and to predict NMR chemical shifts. For crystallographic structures containing multiple chains, only chain A was considered. For each crystallographic structure, the conformation of $NS5B_{\Delta 21}$ was classified as open or closed using two parameters: the inter-subdomain angle and the template channel width. The inter-subdomain angle is the angle formed by the centers of mass of the fingers, palm and thumb NS5B subdomains (as defined by Lesburg *et al.* (2)), and the cutoff value is 70°. The template channel width is defined as the distance between the centers of mass of residues 139 (in the fingers subdomain) and 405 (in the thumb subdomain), and the cutoff value is 20 Å.

Table S5

(a)

Residue	kex (s^{-1})	Δkex (s^{-1})	pB (%)	ΔpB (%)	Δω(^{13}C) (ppm)	ΔΔω(^{13}C) (ppm)	Δω(^{1}H) (ppm)	ΔΔω(^{1}H) (ppm)	χ^2	Reduced χ^2
23	2187	481	*21.5*	*217.7*	*0.20*	*0.73*	*-0.032*	*7.295*	2.659	0.222
71	1398	114	25.9	11.2	0.25	0.04	*-0.064*	*0.241*	3.961	0.330
160	2024	509	3.8	3.4	0.83	0.39	---	---	26.068	2.005
233	*620*	*1418*	*26.4*	*307.7*	*0.13*	*0.24*	*0.041*	*2.025*	4.031	0.336
363	570	117	2.3	0.4	0.59	0.09	---	---	3.232	0.249
432	1502	288	*20.7*	*46.2*	*0.32*	*0.32*	*0.093*	*0.255*	9.818	0.818
462	2675	2068	*0.7*	*0.8*	1.38	0.95	---	---	19.707	1.516
								Total:	69.476	0.799

(b)

Residue	kex (s^{-1})	Δkex (s^{-1})	pB (%)	ΔpB (%)	Δω(^{13}C) (ppm)	ΔΔω(^{13}C) (ppm)	Δω(^{1}H) (ppm)	ΔΔω(^{1}H) (ppm)	χ^2	Reduced χ^2
23	1309	135	*6.1*	*6.6*	0.32	0.17	-0.070	0.050	88.008	0.917
71					0.49	0.26	*0.000*	*316.4*		
160					0.69	0.39	0.090	0.030		
233					0.28	0.14	*0.000*	*115.3*		
363					0.35	0.19	*0.000*	*54.8*		
432					0.55	0.28	*0.030*	*0.110*		
462					0.43	0.25	0.120	0.020		

(c)

Residue	kex (s^{-1})	Δkex (s^{-1})	pB (%)	ΔpB (%)	Δω(^{13}C) (ppm)	ΔΔω(13C) (ppm)	Δω(^{1}H) (ppm)	ΔΔω(^{1}H) (ppm)	χ^2	Reduced χ^2
23	742	262	*14.8*	*75.7*	*-0.23*	*0.51*	---	---	10.015	0.910
71	1570	400	*20.6*	*165.1*	*0.28*	*0.82*	*0.019*	*5.5*	19.318	1.932
160	2266	920	1.3	0.1	3.58	0.41	---	---	6.114	0.556
								Total:	35.447	1.108

(d)

Residue	kex (s^{-1})	Δkex (s^{-1})	pB (%)	ΔpB (%)	Δω(^{13}C) (ppm)	ΔΔω(^{13}C) (ppm)	Δω(^{1}H) (ppm)	ΔΔω(^{1}H) (ppm)	χ^2	Reduced χ^2
23	1074	145	3.6	1.1	0.48	0.08	*0.000*	*197.3*	54.739	1.610
71					0.60	0.11	*0.000*	*21.4*		
160					3.07	0.63	-0.200	0.060		

Table S5. Parameters resulting from fits of models of two-state exchange to methyl-TROSY MQ CPMG relaxation dispersion data. Parameter values and their associated uncertainties, estimated using the covariance matrix method, were obtained using the cpmg_fitd9 software (3). (a, b), apo NS5B$_{\Delta 21}$; (c, d) NS5B$_{\Delta 21}$:filibuvir complex; (a, c) individual-residue fits; (b, d) grouped fits to a common exchange process. kex, exchange rate; pB, population of minor exchanging state; Δω, chemical shift change between states; χ^2, chi-squared goodness of fit measure calculated as $\chi^2 = \sum_i (R_{2,\mathrm{eff}}^{\mathrm{exp}}(i) - R_{2,\mathrm{eff}}^{\mathrm{calc}}(i))^2 / \sigma_i^2$, where $R_{2,\mathrm{eff}}^{\mathrm{exp}}$ and $R_{2,\mathrm{eff}}^{\mathrm{calc}}$ are

experimental and back-calculated $R_{2,eff}$ values constituting the dispersion curves, σ is the experimental error, and *i* runs over all data points fit together; reduced χ^2, χ^2 value divided by the number of degrees of freedom of the fit (number of data points minus number of fit parameters). For individual-residue fits, where ^{1}H $\Delta\omega$ values are given, both ^{1}H and ^{13}C $\Delta\omega$ were allowed to vary; otherwise, ^{1}H $\Delta\omega$ was set to zero. The choice between the two was made based on the result with smaller parameter uncertainties since the difference in goodness of fit was not significant. *Italics* indicate parameters whose uncertainty exceeds the parameter value.

References

1. Han, B., Liu, Y., Ginzinger, S. W., and Wishart, D. S. (2011) SHIFTX2: significantly improved protein chemical shift prediction. *J. Biomol. NMR*. **50**, 43–57
2. Lesburg, C. A., Cable, M. B., Ferrari, E., Hong, Z., Mannarino, A. F., and Weber, P. C. (1999) Crystal structure of the RNA-dependent RNA polymerase from hepatitis C virus reveals a fully encircled active site. *Nat. Struct. Biol.* **6**, 937–43
3. Korzhnev, D. M., Neudecker, P., Mittermaier, A., Orekhov, V. Y., and Kay, L. E. (2005) Multiple-site exchange in proteins studied with a suite of six NMR relaxation dispersion experiments: an application to the folding of a Fyn SH3 domain mutant. *J. Am. Chem. Soc.* **127**, 15602–15611